

Scanning Fluorescence Correlation Spectroscopy for Quantification of the Dynamics and Interactions in Tube Organelles of Living Cells

Joseph D. Unsay⁺,^[a, b, c] Fabronia Murad⁺,^[a] Eduard Hermann,^[b] Jonas Ries,^[d] and Ana J. García-Sáez^{*[a, b]}

Single-molecule spectroscopic quantification of protein-protein interactions directly in the organelles of living cells is highly desirable but remains challenging. Bulk methods, such as Förster resonance energy transfer (FRET), currently only give a relative quantification of the strength of protein-protein interactions. Here, we introduce tube scanning fluorescence cross-correlation spectroscopy (tubeSFCCS) for the absolute quantification of diffusion and complex formation of fluorescently labeled molecules in the mitochondrial compartments. We

determined the extent of association between the apoptosis regulators Bcl-xL and tBid at the mitochondrial outer membrane of living cells and discovered that practically all mitochondria-bound Bcl-xL and tBid are associated with each other, in contrast to undetectable association in the cytosol. Furthermore, we show further applicability of our method to other mitochondrial proteins, as well as to proteins in the endoplasmic reticulum (ER) membrane.

1. Introduction

Most biological processes in the cell are carried out or regulated by direct protein-protein interactions, many of which take place at cellular organelles. To date, various techniques allow detection of protein-protein interaction including a wide array of advanced fluorescence methods.^[1] However, techniques to determine the strength of these interactions and how they are modulated by competing reactions are often lacking, leaving us with a fundamental gap in understanding of how the molecular mechanisms of these interactions lead to function. The quantification of protein association in membranes poses an additional challenge, but can be achieved *in vitro* with acceptable precision and more or less sophisticated membrane models by means of biochemical assays, spectroscopic methods, or mass spectrometry.^[2] Although minimal reconstituted systems offer a chemically controlled environment, they miss the complex composition and dynamics of the cell, which limits the extrapolation to physiological conditions. Thus, quantifica-

tion of the association between organellar proteins in their native environment in the cell is mostly restricted to qualitative and relative analyses, like protein co-localization, immunoprecipitation or Förster resonance energy transfer (FRET),^[3] which hinder a comprehensive understanding of membrane-based cellular interactions.

Fluorescence correlation spectroscopy (FCS) measures the fluorescence fluctuations within the focal volume of a microscope (~0.5 fL) with single molecule sensitivity.^[4] The temporal autocorrelation of the fluorescence intensity trace is fitted with adequate mathematical models to obtain quantitative information about the diffusion and concentration of the fluorescently labeled molecules in the sample. Binding events were often characterized by the huge change in diffusion behavior of fluorescently labeled molecules. However, this is only applicable when the change in diffusion is large (e.g., from very mobile molecules in solution/cytosol to practically immobile proteins when bound to large complexes).^[5] For measuring association events involving similarly sized particles, the change in diffusion behavior is not easily observable.^[6]

To circumvent this challenge, two-color Fluorescence Cross-Correlation Spectroscopy (FCCS) was developed.^[7] The fluorescence fluctuations in two spectral channels are cross-correlated to estimate the fraction of co-diffusing labeled molecules. FCCS has emerged as a robust method to quantify protein bimolecular interactions *in vitro*,^[8] which include studies in model membrane systems like Giant Unilamellar Vesicles (GUVs) and supported lipid bilayers in its linear scanning version.^[9] It can also be applied to cytosolic proteins,^[10] nuclear proteins,^[11] and it has even been successfully used to quantify receptor-ligand interactions on the cell surface of cells,^[12] living fish embryos^[13a] and on the cell membranes of plant cells.^[13b] In conjunction, two-focus scanning FCS (SFCS) is particularly well-suited to measure in microscopically flat membranes. The


[a] J. D. Unsay,⁺ F. Murad,⁺ A. J. García-Sáez
Interfaculty Institute of Biochemistry
University of Tübingen,
Hoppe-Seyler-Str. 4, 72076, Tübingen, Germany
E-mail: ana.garcia@uni-tuebingen.de

[b] J. D. Unsay,⁺ E. Hermann, A. J. García-Sáez
Max Planck Institute for Intelligent Systems
Heisenbergstrasse 3, 70569, Stuttgart, Germany

[c] J. D. Unsay⁺
German Cancer Research Center
Im Neuenheimer Feld 280, 62120, Heidelberg, Germany

[d] J. Ries
European Molecular Biology Laboratory (EMBL)
Meyerhofstrasse 1, 69117, Heidelberg, Germany

[⁺] These authors contributed equally

 Supporting information for this article is available on the WWW under <https://doi.org/10.1002/cphc.201800705>

scanning acquisition protocol allows correcting for membrane movements and minimizing photobleaching,^[9d] as well as allowing for longer measuring times.^[9a,b,14] In addition, the two-focus approach provides absolute values for diffusion constants and concentrations, if the distance between the two foci is known.^[15] However, most cellular organelles adopt a more complex tubular shape, which has limited the use of FCS in these cellular structures.^[16–18]

Here, we have implemented a new method based on SFCS that extends its application to tubular organelles, specifically the mitochondrial inner and outer membranes, as well as the matrix. We have developed suitable data acquisition protocols that are optimized for the complex structure and dynamic nature of mitochondria of living cells, and which also consider the relatively slow motion of molecules in the mitochondrial compartments. In addition, we have tested the appropriateness of different mathematical models for data analysis and identified the optimal models to extract quantitative information from tubular structures. We demonstrate the applicability of the method by quantifying the extent of complex formation between the apoptotic regulators Bcl-xL and tBid at the mitochondrial outer membrane (MOM), and show the potential of the method for other protein complexes and cellular organelles with proof-of-principle measurements of succinyl dehydrogenase complexes at the mitochondrial inner membrane and of mVenus targeted to the endoplasmic reticulum (ER).

2. Results and Discussion

2.1. Optimizing Acquisition Conditions and Finding the Appropriate Diffusion Model

Mitochondria are dynamic organelles that appear as a tubular network in most cells and therefore are not amenable for standard point FCS. To address the dynamics of these networks, we took inspiration on SFCS applied to GUVs^[9b–e] and derived new, optimized acquisition protocols. We repeatedly scanned the focal volume perpendicular to the in-focus mitochondrial tube (Figure 1A). Due to the slow diffusion of proteins at mitochondrial compartments, we demonstrated that 500 s acquisition time is required to collect sufficient fluorescence fluctuation events. The resulting data can then be used to make a pseudo image by stacking one scan after the other (Figure S1A in the Supporting Information), where the signal from a single mitochondrion can be selected and aligned. This corrects the position changes of the mitochondrion during the acquisition time (Figure S1B) and reduces the residence time of the fluorophores in the focal volume, thereby minimizing photobleaching effects. Since the diameter of mitochondria (~0.5 μm , Figure S2A) is comparable to the length of the z axis of the confocal detection volume, we examined the effect of the focal volume size on the quality of the autocorrelation curves by acquiring SFCS curves for GFP targeted at the mitochondrial matrix, and outer and inner membranes at different pinhole apertures to include the whole mitochondrion. We found that

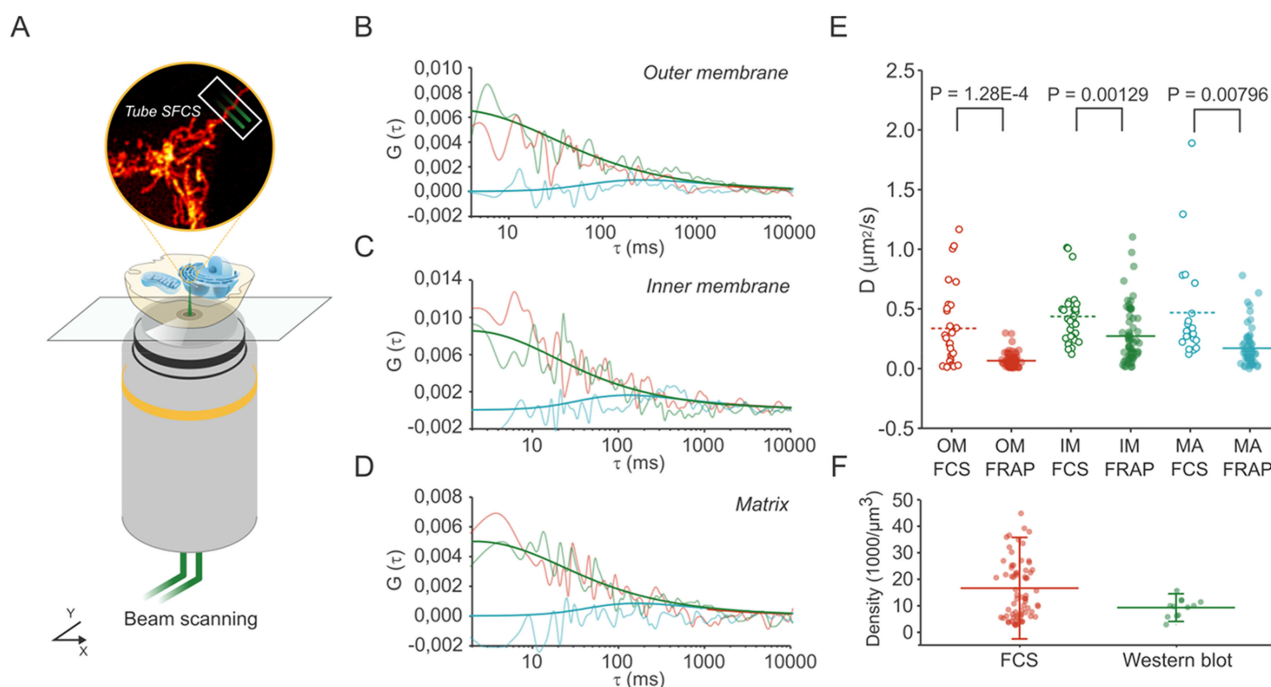


Figure 1. tubeSFCS to measure the diffusion coefficient and concentration of mitochondria-targeted proteins. (A) Scheme of tubeSFCS acquisition strategy using two-focus linear scanning across a mitochondrial tube in living cells. (B), (C) and (D) Red and green curves represent the autocorrelation of the fluctuating signal as measured for each of the two foci. The blue curve represents the spatial cross-correlation of the signals measured across the two foci fitted globally with a two-focus model (see Table 1 and Equation S15 in the Supporting Information). (E) Comparison of the diffusion coefficient calculated for GFP targeted to the mitochondrial matrix (MA), the outer membrane (OM) or the inner membrane (IM) using tubeSFCS (FCS) or FRAP. (F) Comparison of the concentration of mito-GFP calculated with tubeSFCS (FCS) and quantitative western blot.

the data obtained with 1 airy unit (AU), which should be sufficient to capture the whole mitochondrial section in one scan (Figure S2C), produced the best results. The values for concentration and diffusion time were less noisy and less dispersed and selected these conditions for further measurements.

Whereas scanning FCS is able to measure molecular diffusions on membranes, tubeSFCS expand the capability to the tubular nature of the membrane organelle as well as the complex cristae invaginations of the inner mitochondrial membrane. These special characteristics of the underlying geometry in which the fluorescent proteins or lipids diffuse require different mathematical data handling models that take the consequences of mitochondrial shape on diffusion into account. To identify an appropriate mathematical model to fit the autocorrelation curves, we compared the performance of different diffusion models (Table 1) on the FCS data acquired and simulated the mobility of GFP targeted to the mitochondrial matrix, as well as the inner and outer membranes. (Supporting Information Section 3, Figures S3 and S4).

Previous studies have used the 3D Diffusion Model stating its simplicity and robustness in analyzing diffusion of fluorophores in the mitochondria.^[16] On the other hand, we have extensively used the 2D Elliptical Gaussian model for SFCS in GUVs.^[9c,e] In this model, the particles are diffusing freely on the plane perpendicular to the scanning path. In 2000, Generich and Schild presented a solution to diffusion in small tubular cytosolic compartments.^[17] We adapted their solution to the case of the mitochondria, where the diffusion in the x-axis is free (axis of the mitochondria), in the z-axis is confined (optical axis), and non-existent in the y-axis (scanning path) to give the 2D Confined Diffusion equation in Table 1.

Generich and Schild also presented limitations and simplifications of the model. In one case, they derived the limit of 2D diffusion model $G_{xz}(\tau)$. They calculated what should be the ratio (Z) between the diameter of the compartment (d_{mito}) and the axial extension of the diffusion volume (ω_z) so that fluctuations in the z-axis can be neglected. They derived this limit to be $Z < 0.833$. In the case of the mitochondria, the measured diameter was biggest when GFP was targeted to the outer membrane at $0.46 \pm 0.1 \mu\text{m}$ (Figure S2B). The resulting ratio is less than the limit 0.833. Thus, in SFCS of mitochondria,

another possible model would be to not consider fluctuations in the z-axis, making it an apparent 1D free diffusion

In view of these numerous possibilities, we fitted the experimental data from SFCS with these different models: 1D free diffusion (1D Free), 2D Free with Gaussian Detection (2D Gauss), 3D free diffusion (3D Free), and both cases of the 2D confined diffusion from Generich and Schild (Case 1 where $Z \in [0, 3.1]$ is denoted as "2D Conf A" and Case 2 where $Z \in [3.1, 8]$ is denoted as "2D Conf B"). Figure S3A shows these fittings for the outer membrane, inner membrane and matrix. Figure S3B shows the residual of the fittings for each model. Figure S3C shows the distribution of the calculated diffusion times for each model, in which 3D Free shows the highest deviation. Compared to the other models 2D Conf A and 2D Conf B seems to estimate a higher number of particles for the same curves (Figure S3D). However, the sum of square residuals indicate that the fitting of each curve is equally good or equally bad no matter which model we used.

To further check and eliminate possible candidate models, we fitted a simulated autocorrelation curve for the mitochondrial surface and matrix using the different models. We first used smoldyn,^[19] a particle-based simulator, to generate fluorescence fluctuation traces and then auto-correlated these traces using a multi-tau algorithm^[20] code written by Zdenek Petrsek. Figure S4 A and B show the simulated FCS curves and the residuals.

We then compared the diffusion coefficient from the fitting vs. the theoretical, simulated diffusion coefficient (Figure S2C). Compared to the other models, only the 1D Free diffusion model is in good agreement between the simulated data and the calculated result from the fitting. From the fluctuation traces, we also calculated the average number of particles in the detection volume (N), and compared this with the actual number of particles introduced in the simulations (Figure S4D). We showed that the 2D Conf A overestimates the N from the simulations. With these results in mind, we narrowed down our choices to two candidate models: 1D Free and 2D Gauss.

We employed Bayesian Interaction Criterion (BIC) to determine if there is any difference in these two models. BIC is a criterion for model selection among a finite set of models. In fitting different models, it is possible to increase likelihood (and therefore goodness of fit) by adding more parameters, but this could lead to overfitting.^[21] BIC resolves this by introducing a

Table 1. Diffusion Models for FCS.

Model	Equation
3D Free Diffusion (3D Free)	$G_{3D}(\tau) = \frac{1}{N} \left(1 + \frac{\tau}{\tau_D}\right)^{-1} \left(1 + \frac{\tau}{5^2 \tau_D}\right)^{-1/2}$
2D Elliptical Gaussian (2D Gauss)	$G_{2DGauss}(\tau) = \frac{1}{N} \left(1 + \frac{\tau}{\tau_D}\right)^{-1/2} \left(1 + \frac{\tau}{5^2 \tau_D}\right)^{-1/2}$
1D Free Diffusion (1D Free)	$G_{1D}(\tau) = \frac{1}{N} \left(1 + \frac{\tau}{\tau_D}\right)^{-1/2}$
2D Confined Diffusion (2D Conf)	$G_{xz*} = \frac{1}{N} \left(1 + \frac{\tau}{\tau_D}\right)^{-1/2} g_{z*}(\tau)$ $g_{z*}(\tau) = \begin{cases} 1 + \frac{Z}{45} (1 - 0.1004Z^2 + 0.00361Z^4) \exp\left(-\left(\frac{\pi}{5\sqrt{Z}}\right)^2 \frac{\tau}{\tau_D}\right), & Z \in [0, 3.1] \\ 1 + \left(\frac{Z}{\sqrt{\pi}} - 1\right) \exp\left(-\left(\frac{0.833\pi}{5\sqrt{Z}}\right)^2 \frac{\tau}{\tau_D}\right) \left(1 + \frac{\tau}{5^2 \tau_D}\right)^{-1/2}, & Z \in [3.1, 8] \end{cases}$ $Z = \frac{d_{\text{mito}}}{\omega_z}$

penalty for the number of parameters in the model (Equation 1).

$$BIC = n^* \ln\left(\frac{SSR}{n}\right) + k \ln(n) \quad (1)$$

where n is the number of points being fitted by the model, SSR is the sum of square residuals and k is the number of fitting parameters. The difference between the BIC of the models for each experimental curve is then calculated. The difference for 1D Free and 2D Gauss falls in the range of 0–52, with medians of 4 for the outer membrane (44 curves analyzed), 12 for the inner membrane (29 curves analyzed) and 4 for the Matrix (40 curves analyzed). For more details, including BIC differences for simulated curves, see Table S1 in the Supporting Information. This difference indicates a positive evidence against the model with the higher BIC value (in all cases, against 2D Gauss model).^[22]

We can then say that 1D free diffusion model, which approximates diffusion to random linear mobility within the mitochondrial tube, was the most appropriate to describe the diffusion of particles in mitochondria of living cells, regardless of the mitochondrial compartment. It is interesting to note, that recently, the group of Elson published a preprint in bioRxiv detailing FCS on membrane nanotubes.^[18] They discuss the implication of the size of the tube with respect to a 1D Free and 2D Free diffusion model, stating that in tubes, the fitting is an intermediate between these two models, however, they have not shown an analytical solution to the correlation curve.

In the following sections, all experimental correlation curves were fitted with the 1D Free diffusion model.

Finally, we also compared the quality of the data obtained with one- or two-focus SFCS and found that the latter, which adds the spatial cross-correlation of the fluorescence signal between the two foci, provided less dispersed and more accurate data (Figure S5D) and was selected for tubeSFCS (Figure 1B–D).

2.2. Measuring Diffusion and Concentration in the Mitochondria of Living Cells

To ensure that tubeSFCS reliably provides accurate values for the concentration and diffusion coefficient of the labeled molecules of interest, we compared results from alternative, independent and well-established methods. In the case of mobility, we compared the results obtained by tubeSFCS (Figures 1B–D and S5A,B in the Supporting Information) for GFP-targeted to the mitochondrial matrix, as well as to the inner and outer membranes with the diffusion coefficients calculated for the same proteins from experiments of fluorescence recovery after photobleaching (FRAP) (Figure S5C). As shown in Figure 1E, the values obtained with both methods in all mitochondrial compartments were in good agreement, with the FCS data providing slightly higher values than FRAP and a significant difference in the case of the MOM. These discrepancies are likely due to fact that FCS only accounts for

the mobile fraction of the molecules, while FRAP also considers immobile particles. Additional challenges associated with FRAP, which include mitochondria movement during acquisition and the non-trivial conversion of half time to diffusion coefficient as previously discussed,^[23] are also likely to make a contribution. Remarkably, the diffusion coefficients calculated by tubeSFCS here are in very good agreement with the values obtained by super resolution single molecule tracking.^[24]

To confirm that the concentration values calculated with tubeSFCS in individual mitochondria were in line with protein levels estimated by other methods, we compared them with quantitative western blot analysis (Figure S6). We found that the average number of mitoGFP particles per mitochondrial volume was of the same order of magnitude, with significantly larger dispersion in the case of tubeSFCS (Figure 1F). This is reasonable, because tubeSFCS data provides protein concentrations for single mitochondria in individual cells, while western blot is a bulk technique that provides average values for the whole cell population in the sample and therefore misses both inter- and intra-cellular heterogeneities.

2.3. Measuring Interaction Using Two-Color FCCS: tBid and Bcl-xL Binding in Live Cells

The ability of tubeSFCS to calculate absolute quantities allows the use of the two-color version, tubeSFCCS, to directly quantify molecular interactions between proteins targeted to mitochondria in living cells, providing absolute values about the number of proteins engaged in complexes. As proof of principle, we examined the interaction between Bcl-xL and tBid, which are representative anti- and pro-apoptotic members of the Bcl-2 family, respectively. During apoptosis, tBid activation leads to MOM permeabilization, a key step in cell death execution. Bcl-xL inhibits apoptosis by binding to tBid and blocking its pro-death function, and as a result, the association between tBid and Bcl-xL is a key factor for determining cell fate. Because many cancer cell increase the levels of prosurvival Bcl-2 homologs like Bcl-xL to escape cell death, disrupting their association with tBid-like molecules is a target for drug discovery.^[25]

To avoid interference with the endogenous, unlabeled proteins, we generated Bcl-xL/Bid DKO MEFs from Bid knockout MEFs using the CRISPR/Cas9 System (See Experimental Section in the Supporting Information and Figure S7) and transfected them transiently with tBid-GFP and mCherry-Bcl-xL. We then measured point FCCS in the cytosol and one-focus tubeSFCCS with pulsed interleaved excitation (PIE)^[26] in the mitochondria of single cells (Figure 2A–C). Although the two-focus mode is superior to the one-focus mode in measuring the diffusion coefficient (see previous section), limitations from our microscope and data acquisition set up did not allow to do PIE together with two-focus mode. In Figure S5E, it is shown that the number of particles N (which is the basis for the calculation of the percentage of cross-correlation (%CC)) are not significantly different between the one-focus and two-focus fitting.

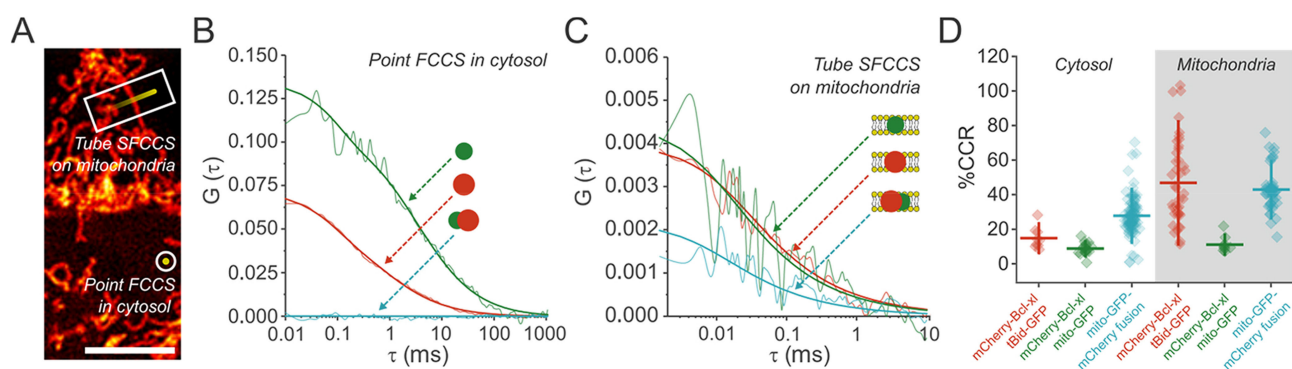


Figure 2. tubeSFCCS for the quantification of the extent of complex formation between mitochondrial proteins. (A) Scheme of acquisition strategies of point FCCS and one-focus scanning FCCS with PIE illumination for the quantification of protein interactions in the cytosol and mitochondrial tubes, respectively, in living cells. (B) Representative auto- (red and green) and spectral cross- (blue) correlation curves of point FCCS performed in the cytosol of Bid/Bcl-xL double knockout MEFs transfected with tBid-GFP and mCherry-Bcl-xL and fitted with a 3D free diffusion model (equation 13). The zero amplitude of the blue cross-correlation curve indicates no interaction. (C) Representative auto- (red and green) and spectral cross- (blue) correlation curves of tubeSFCCS performed on the mitochondria of Bid/Bcl-xL double knockout MEFs transfected with tBid-GFP and mCherry-Bcl-xL and fitted with a 1D free diffusion model (See Supporting Information). The positive amplitude of the blue cross-correlation curve indicates interaction between the proteins when they are located at the MOM. (D) Percentage cross correlation with respect to the red channel (%CCR) calculated from measurements performed in the cytosol and mitochondria of Bid/Bcl-xL double knockout MEFs transfected with either tBid-GFP/mCherry-Bcl-xL (red) [N = 51 (cytosol), N = 102 (mitochondria)], mCherry-Bcl-xL/mito-GFP (green) [N = 65 (cytosol), N = 24 (mitochondria)] acting as negative control (see Figure S10), or mito-GFP-mCherry fusion (blue) [N = 109 (cytosol), N = 48 (mitochondria)] acting as positive control.

We compared the percentage cross-correlation (%CC), which provides information about the fraction of fluorophores co-diffusing as complexes, with a negative control (mito-GFP and mCherry-Bcl-xL) and a positive control (mito-GFP-mCherry) of interaction. Figure 2D shows that complex formation (proportional to %CC) between tBid-GFP and mCherry-Bcl-xL was significantly higher and favored in the membrane environment of the MOM compared with the cytosol, in agreement with the results obtained previously in GUVs.^[9c,e]

Note that the average %CC between tBid-GFP and mCherry-Bcl-xL is close to 50% and comparable to that of the positive control of fused GFP and mCherry. The positive control gives estimation of the maximum CC possible in our system and accounts for incomplete maturation of both GFP and mCherry, as well as the partial overlap of the detection focal volumes in the green and the red channels. These effects also set the maximum possible CC in the tBid-GFP/mCherry-Bcl-xL. The larger dispersion of the individual data points, also towards higher %CC values, could be due to potential oligomer formation, which cannot be excluded in the context of the cell.^[9e,27] It could also be related to different “primed-for-death” state of the individual cells, which could affect the heterogeneity of Bcl-xL localization and association with BH3-only proteins at the single cell level.^[28] Altogether, these results indicate that on average, when in mitochondria, tBid and Bcl-xL molecules have a very high affinity for each other and are engaged in complexes together, similar to the interactions measured *in vitro*.^[9c] Although a previous study based on FRET measurements calculated the relative affinities between BH3-only proteins and prosurvival Bcl-2 proteins in cells,^[29] it failed to estimate the actual extent of complex formation between the different proteins. In addition, the overexpression conditions needed for FRET measurements are likely to affect the fraction of proteins bound in the cells, in contrast to the low

expression levels used in our study. The fact that practically all tBid and Bcl-xL molecules are bound in complexes at mitochondria has consequences for drug design, which could likely be improved by considering the presence of the lipid membrane environment.

2.4. Further Applications

The framework developed here for tubeSFCCS can be easily extended to other compartments of the mitochondria as well as other intracellular organelles with tubular shape. As proof-of-principle, we demonstrated that it can also be used to detect interactions between labeled proteins in the mitochondrial matrix such as the succinyl dehydrogenase (Figure S8) and to measure protein mobility and concentration of labeled proteins at the ER membrane (Figure S9).

3. Conclusions

Our study provides for the first time the evidence that the extent of complex formation between two interacting proteins directly in the mitochondria of living cells and presents a new tool for the absolute quantitative analysis of protein concentration, diffusion and interactions in the tubular organelles of living cells. We demonstrate the value of this enabling method by determining that the apoptosis regulators tBid and Bcl-xL bind with very high affinity specifically at mitochondria, but not in the cytosol, which has implications for the optimization of anti-cancer drugs targeting this interaction.

Acknowledgements

This project was funded by the European Research Council (ERC-StG 309966). J.D.U. was partially supported by the German Cancer Research Center and the Max Planck Society. The authors thank Britta Liebler, Sabine Schäfer and Carolin Stegmüller for technical assistance. Aida Pena Blanco, Raquel Salvador Gallego, Begona Ugarte Uribe, Stephanie Bleicken, John Danial and Monika Zelman for useful discussions. The authors also thank the sources of different materials as stated in the Experimental Section in the Supporting Information. Finally, we thank Cornelia Grimm and the FACS Core Facility at the Universitätsklinikum Tübingen for the cell sorting services.

Conflict of Interest

The authors declare no conflict of interest.

Keywords: biophysics · fluorescence correlation spectroscopy · membranes · mitochondrial proteins · protein-protein interaction

- [1] a) L. Sandord, A. Palmer in *Methods in Enzymology Vol. 589* (Eds: R. B. Thompson, C. A. Fierke), Elsevier Academic Press, Inc., San Diego, CA, USA **2017**, pp. 1–49; b) F. J. Meyer-Almes, *Methods Appl. Fluoresc.* **2017**, *5*, 042002; c) S. M. Hashemi, A. E. C. Meijering, W. H. Roos, G. J. L. Wuite, E. J. G. Peterman in *Methods in Enzymology, Vol. 582* (Eds.: M. Spies, Y. R. Chemla), Elsevier Academic Press, Inc., San Diego, CA, USA, **2017**, pp. 85–119; d) N. Loren, J. Hagman, J. K. Jonasson, H. Deschout, D. Bernin, F. Cella-Zanacchi, A. Diasporo, J. G. McNally, M. Ameloot, N. Smisdom, M. Nyden, A. M. Hernasson, M. Rudemo, K. Braeckmans, *Q. Rev. Biophys.* **2015**, *48*, 323–387.
- [2] a) H. Jung, A. D. Robison, P. S. Cremer, *J. Struct. Biol.* **2009**, *168*, 90–94; b) S. Bleicken, M. Otsuki, A. J. García-Saez, *Curr. Protein Pept. Sci.* **2011**, *12*, 691–698; c) S. Hunke, V. S. Müller in *Protein Interactions* (Eds: J. Cai, R. E. Wang), InTech, **2012**, DOI: 10.5772/38069; d) Y. Miao, T. A. Cross, *Curr. Opin. Struct. Biol.* **2013**, *23*, 919–928; e) G. Siligardi, R. Hussain, S. G. Patching, M. K. Phillips-Jones, *Biochim. Biophys. Acta Biomembr.* **2014**, *1838*, 34–42; f) A. S. Khadria, A. Senes Pept. Sci. **2015**, *104*, 247–264.
- [3] a) F. Fricke, M. S. Dietz, M. Heilemann *ChemPhysChem* **2014**, *16*, 713–721; b) Q. Liu, B. Leber, D. W. Andrews *Cell Cycle* **2012**, *11*, 3536–3542; c) V. Fernández-Dueñas, J. Llorente, D. O. Borroto-Escuela, L. F. Agnati, C. I. Tasca, J. Fuxe, F. Ciruela, *Methods* **2012**, *57*, 467–472.
- [4] a) D. Magde, E. Elson, W. W. Webb, *Phys. Rev. Lett.* **1972**, *29*, 705–708; b) R. Rigler, Ü. Mets, J. Widengren, P. Kask, *Eur. Biophys. J.* **1993**, *22*, 16–175.
- [5] a) T. Weidemann, M. Wachsmuth, T. A. Knoch, G. Müller, W. Waldeck, J. Langowski, *J. Mol. Biol.* **2003**, *334*, 229–240; b) Z. W. Zhao, M. D. White, Y. D. Alvarez, J. Zenker, S. Bissiere, N. Plachta *Nat. Protoc.* **2017**, *12*, 1458–1471.
- [6] Change in diffusion time needs to be by a factor of 1.6, which is about an 8-fold change in molecular weight. U. Meseth, T. Wohland, R. Rigler, H. Vogel *Biophys. J.* **1999**, *76*, 1619–1631.
- [7] a) P. Schwillie, F.-J. Meyer-Almes, R. Rigler, *Biophys. J.* **1997**, *72*, 1878–1886; b) K. Bacia, P. Schwillie, *Nat. Protoc.* **2007**, *2*, 2842–2856.
- [8] a) S. Milles, E. A. Lemke, *Angew. Chem. Int. Ed.* **2014**, *53*, 7364–7367; *Angew. Chem.* **2014**, *126*, 7492–7496; b) F. H. Moonschi, A. K. Effinger, X. Zhang, W. E. Martin, A. M. Fox, D. K. Heidary, J. E. DeRouchey, C. I. Richards, *Angew. Chem. Int. Ed.* **2014**, *54*, 481–484
- [9] a) J. Ries, S. Chiantia, P. Schwillie, *Biophys. J.* **2009**, *96*, 1999–2008; b) J. Ries, P. Schwillie, *Biophys. J.* **2006**, *91*, 1915–1924; c) A. J. Garcia-Saez, J. Ries, M. Orzaez, E. Perez-Paya, P. Schwillie, *Nat. Struct. Mol. Biol.* **2009**, *16*, 1178–1185; d) J. D. Unsay, A. J. Garcia-Saez in *Membrane Biogenesis: Methods and Protocols* (Eds: D. Rapaport, J. M. Herrmann), Humana Press, **2013**, pp. 185–205; e) S. Bleicken, A. Hantusch, A. K. K. Das, T. Frickey, A. J. Garcia-Saez, *Nat. Commun.* **2017**, *8*, 73.
- [10] a) C. I. Maeder, M. A. Hink, A. Kinkhabwala, R. Mayr, P. I. Bastiaens, M. Knop, *Nat. Cell Biol.* **2007**, *9*, 1319; b) B. D. Slaughter, J. W. Schwartz, R. Li, *Proc. Mont. Acad. Sci.* **2007**, *104*, 20320–20325; c) S. A. Kim, K. G. Heinze, P. Schwillie, *Nat. Methods* **2007**, *4*, 963–973.
- [11] a) N. Baudendistel, G. Müller, W. Waldeck, P. Angel, J. Langowski, *ChemPhysChem* **2005**, *6*, 984–990; b) A. Pernuš, J. Langowski, *PLoS One* **2014**, *10*, e0123070; c) M. Tiwari, S. Oasa, J. Yamamoto, S. Mikuni, M. Kinjo *Sci. Rep.* **2017**, *7*, 4336.
- [12] a) J. Sankaran, M. Manna, L. Guo, R. Kraut, T. Wohland, *Biophys. J.*, **2009**, *97*, 2630–2639; b) R. M. Dörlich, Q. Chen, P. N. Hedde, V. Schuster, M. Hippler, J. Wesslowski, G. Davidson, G. U. Nienhaus, *Sci. Rep.* **2015**, *10149*.
- [13] a) J. Ries, S. R. Yu, M. Burkhardt, M. Brand, P. Schwillie, *Nat. Methods* **2009**, *6*, 643–645; b) X. Li, J. Xing, Z. Qiu, Q. He, J. Lin, *Mol. Plant* **2016**, *9*, 1229–1239.
- [14] M. A. Digman, C. M. Brown, P. Sengupta, P. W. Wiseman, A. R. Horwitz, E. Gratton, *Biophys. J.* **2005**, *89*, 1317–1327.
- [15] a) T. Dertinger, V. Pacheco, I. von der Hocht, R. Hartmann, I. Gregor, J. Enderlein, *ChemPhysChem* **2007**, *8*, 433–443; b) T. Dertinger, A. Loman, B. Ewers, C. B. Müller, B. Krämer, J. Enderlein, *Opt. Express* **2008**, *16*, 14353–14368. c) J. W. Krieger, A. P. Singh, N. Bag, C. S. Garbe, T. E. Saunders, J. Langowski, T. Wohland, *Nat. Protoc.* **2015**, *10*, 1948–1974.
- [16] a) W. J. Koopman, M. A. Hink, S. Verkaart, H. J. Visch, J. A. Smeitink, P. H. Willems, *Biochim. Biophys. Acta* **2007**, *1767*, 940–947; b) P. H. Willems, H. G. Swarts, M. A. Hink, W. J. H. Koopman in *Methods in Enzymology Vol. 456* (Eds.: W. S. Allison, I. E. Sheffler), Academic Press, **2009** pp. 287–302.
- [17] A. Gennerich, D. Schild, *Biophys. J.* **2000**, *79*, 3294–3306.
- [18] Y. Jiang, A. Melynikov, E. E. Elson, *bioRxiv* **2017**, DOI: <https://doi.org/10.1101/134742>
- [19] S. S. Andrews, N. J. Addy, R. Brent, A. P. Arkin, *PLoS Comput. Biol.* **2010**, *6*, e1000705.
- [20] Z. Petrasek, J. Ries, P. Schwillie in *Methods in Enzymology Vol. 472* (Eds.: Nils G. Walter), Academic Press, **2010**, pp. 317–343.
- [21] a) G. Schwarz, *Ann. Stat.* **1979**, *6*, 461–464; b) E. Wit, E. van den Heuvel, J.-W. Romeijn, *Statistica Neerlandica* **2012**, *66*, 217–236.
- [22] R. E. Krass, A. E. Raftery *J. Am. Stat. Assoc.* **1995**, *90*, 773–795
- [23] a) R. C. Calizo, S. Scarlata, *Biochemistry* **2012**, *51*, 9513–9523; b) T. J. Stasevich, F. Mueller, A. Michelman-Ribeiro, J. R. Knutson, J. G. McNally *Biophys. J.* **2010**, *99*, 3093–3101; c) K. Mitra, J. Lippincott-Schwartz in *Current Protocols in Cell Biology*, Wiley, Hoboken, **2010**, Unit.4.25, 1–21; d) A. Partikian, B. Ölveczky, R. Swaminathan, Y. Li, A. S. Verkman, *J. Cell Biol.* **1998**, *140*, 821–829.
- [24] T. Appelhans, C. P. Richter, V. Wilkens, S. T. Hess, J. Piehler, K. B. Busch, *Nano Lett.* **2012**, *12*, 610–616.
- [25] S. Cory, A. W. Roberts, P. M. Colman, J. M. Adams, *Trends in Cancer* **2016**, *2*, 443–460.
- [26] B. K. Muller, E. Zaychikov, C. Brauchle, D. C. Lamb, *Biophys. J.* **2005**, *89*, 3508–3522
- [27] a) Y. Wang, R. Cao, D. Liu, A. Chervin, J. Yuan, J. An, Z. Huang, *Biochem. Biophys. Res. Commun.* **2007**, *361*, 1006–1011; b) S. Rajan, M. Choi, Q. T. Nguyen, H. Ye, W. Liu, H. T. Toh, C. B. Kang, N. Kamariah, C. Li, H. Huang, C. White, K. Baek, G. Grüber, H. S. Yoon, *Sci. Rep.* **2015**, *5*, 10609; c) S. Shivakumar, M. Kurylowicz, N. Hirmiz, Y. Manan, O. Friaa, A. Shamas-Din, P. Masoudian, B. Leber, D. W. Andrews, C. Fradin, *Biophys. J.* **2014**, *106*, 2085–2095.
- [28] a) M. Certo, V. Del Gaizo Moore, M. Nishino, G. Wei, S. Korsmeyer, S. A. Armstrong, A. Letai, *Cancer Cell* **2006**, *9*, 351–365; b) J. Lopez, S. W. G. Tait, *Br. J. Cancer* **2015**, *112*, 957–962; c) J. Le Pen, M. Laurent, K. Sarosiek, C. Vuillier, F. Gautier, S. Montessuit, J. C. Martinou, A. Letai, F. Braun, P. P. Juin, *Cell Death Dis.* **2016**, *7*, e2083
- [29] A. Aranovich, Q. Liu, T. Collins, F. Geng, S. Dixit, B. Leber, D. W. Andrews, *Mol. Cell* **2012**, *45*, 754–763.

Manuscript received: July 20, 2018
Version of record online: October 18, 2018